

Chapter 9

Fractional SEIR Model for Modelling the Spread of COVID-19 in Namibia



Samuel M. Nuugulu, Albert Shikongo, David Elago, Andreas T. Salom, and Kolade M. Owolabi

Abstract In this chapter, a fractional SEIR model and its robust first-order unconditionally convergent numerical method is proposed. Initial conditions based on Namibian data as of 4 July 2020 were used to simulate two scenarios. In the first scenario, it is assumed that the proper control mechanisms for kerbing the spread of COVID-19 are in place. In the second scenario, a worst-case scenario is presented. The worst case is characterised by ineffective COVID-19 control mechanisms. Results indicate that if proper control mechanisms are followed, Namibia can contain the spread of COVID-19 in the country to a lowest level of 1, 800 positive cases by October 2020. However, if no proper control mechanisms are followed, Namibia can hit a potentially unmanageable level of over 14, 000 positive cases by October 2020. From a mathematical point of view, results indicate that the fractional SEIR model and the proposed method are appropriate for modelling the chaotic nature observed in the spread of COVID-19. Results herein are fundamentally important to policy and decision-makers in devising appropriate control and management strategies for curbing further spread of COVID-19 in Namibia.

Keywords Fractional calculus · Fractional SEIR model · COVID-19 · Well-posedness · Numerical methods · Stability analysis

S. M. Nuugulu (✉) · A. Shikongo · D. Elago
Department of Mathematics, University of Namibia, Private Bag 13301, Windhoek, Namibia
e-mail: snuugulu@unam.na

A. Shikongo
e-mail: ashikongo@unam.na

D. Elago
e-mail: delago@unam.na

A. T. Salom
CERENA-Polo FEUP, Faculty of Engineering, University of Porto, Porto, Portugal
e-mail: andreas.s@fe.up.pt

K. M. Owolabi
Department of Mathematical Sciences, Federal University of Technology,
Akure, Ondo State, Nigeria
e-mail: kmowolabi@futa.edu.ng

Mathematics Subject Classification 92B05 · 65D15 · 92D25 · 45F05 · 91G50 · 74S40

Introduction

It is now common knowledge that towards the end of the year 2019 a severe acute respiratory syndrome coronavirus 2 (SARS-CoV-2) emerged in a Wuhan City of China. In [1, 2], for example, it is mentioned that COVID-19 infections are transmitted from one person to the other primarily through saliva droplets or charges from the noses of infected persons when coughing or sneezing, or physical contacts with an infected person and touching of infected surfaces. The World Health Organisation (WHO) declared the new coronavirus disease a public health emergency of international concern on 31 January 2020. By March 2020, the disease had already spread to the rest of the world in a very shorter period of time. Thus, the WHO on the 11 March 2020 declared COVID-19 a global pandemic. Since then, COVID-19 has been claiming many lives on a daily basis and currently (as of 11 July 2020 (14:00 GMT +8)) the hard-hit countries are San Marino with more than 12,380 deaths, Belgium with over 843 deaths, Andorra with over 672 deaths, followed by the UK with over 656 deaths.

COVID-19 is a highly contagious viral disease that is perpetually imposing severe burdens on public health and economies and has thus created chaos across the globe see for example [2–4] and references therein. Since there exists no clinically tested vaccine or proper medication for treating COVID-19, most governments across the world have drawn their attentions to stiffening of precautionary measures such as lockdowns, social distancing protocols, self-isolations, quarantines as well as enforcing basic public health practices of regular washing and sanitisation of hands to help control further spread of the virus, see for example [2, 5]. In Namibia, President Hage Geingob declared a state of emergency on the 17 March 2020 and stipulated some unprecedented measures to help curb further spreading of COVID-19 in the country.

In view of the above-mentioned developments, models for studying dynamical behaviour of COVID-19 have been developed. For instance, Kassa et al. in [6] formulated and analysed a COVID-19 mathematical model with model parameters estimated from available COVID-19 data. The authors' investigation involved a backward bifurcation analysis which is believed to arise when recovered individuals do not develop permanent immunity for the disease, i.e., ($R_o = 1$) and disappear in the absence of re-infection ($R_o < 1$). Fanelli and Piazza in [7] analysed and forecasted the spread of COVID-19 in China, Italy and France using a simple day-lag map points of a simple susceptible-infected-recovery-death (SIRD) integer-orders model.

Mishra et al. in [2] developed a three special compartmental quarantine models, susceptible-immigrant-home isolation-infectious-hospital quarantine-recovered (SIR) model. The authors performed numerical simulations and concluded that hospitals quarantine and home isolations are indispensable forces to control spread of the

virus in the absence of treatment and vaccine. Postnikov in [4] studied the dynamics of COVID-19 using a simple susceptible-infectious-recovered (SIR) integer-order model proposed by Kermack and McKendrick in [4]. The author applied the sequential reduction of the SIR to a logistic regression-based equation and applied the resultant model to validating the COVID-19 recent data reported by the European Centre for Disease Prevention and Control.

Ullah and Khan [8] also developed a new mathematical transmission model to explore the transmission dynamics and impact of non-pharmaceutical control of the COVID-19 pandemic in Pakistan. In the first instance, they developed their model without optimal control variables and estimated the model parameters from the reported cases using a nonlinear least square curve fitting technique. In the second case, after reformulating the model, they added two time-dependent control variables, i.e., quarantine, hospitalisation and self-isolation interventions for the infected individual. They reported that their model outputs are in good agreement with the COVID-19 confirmed cases in Pakistan. The infection horizons of COVID-19 estimation using a data-driven approach and an SIR model with a time varying disease transmission rate are studied in [9] and [10], respectively. Moreover, Manotosh et al. in [5] formulated a model of integer order to study the dynamical behaviour of the spread of COVID-19 by quantifying the basic reproductive number to help predict and control further the spread of COVID-19 by introducing quarantine and governmental measures components in the model.

The theory of fractional calculus is more than three centuries old just like classical integer-order calculus, but it was not popular in science [11] and engineering field [12–14] and recent discoveries of fractal geometries in different scientific fields of applications such as finance, love dynamics as well as disease modelling, see for example [15–20] and references therein have justified that fractional calculus-based models are appropriate for handling real-world phenomena better than their integer-order counterparts.

Fractional calculus epidemiological models provide a general version of the integer-order epidemiological models by replacing integer-order derivatives with corresponding non-integers-order derivatives. Since fractional differential operators are non-local and are often characterised by power processes [18], fading memories [15] as well cross-overs [14] such features make them appropriate in dealing with dynamical real-life phenomena, see for example [15, 17, 18]. Though these features until recently have only been commonly observed in stock price dynamics, underground water modelling, etc., (see for example [17, 18, 21–23] and reference therein), the extension of fractional calculus in this chapter and also in other recent work in [15, 16, 24, 25] to modelling the chaotic nature of the spread of COVID-19 is well appropriate.

Zhang et al. in [25] applied fractional differential equations in modelling the dynamics and mitigation scenarios of COVID-19 for the first time in China. The authors proposed and applied a time-dependent susceptible-exposed-infectious-recovered (SEIR) model to fit and predict the time series of COVID-19 for three months (22 December 2019 to 22 March 2020) data from China. Their validated

SEIR model was then applied further to predict the dynamic behaviour in Japan, Italy, South Korea and the USA.

Atangana in [16] also applied new fractional operators to modelling the spread of COVID-19 as well as to investigating the effect of governments' lockdown protocols. The author considered the possibility of infection of medical personnels by dead bodies during the postmortem procedures or direct contact during the funeral arrangements, removed the transmission rate from dead bodies and incorporated lockdown and social distancing effects using the next generation matrix. Their results indicate that zero basic reproductive number can be achieved if lockdown recommendations are observed properly.

In [15], Alkahtani and Alzaid investigated the stability conditions for a numerical method based on Lagrange polynomial for fractional-orders epidemiological model with eight compartments. Another fractional derivative-based model was also formulated by Khan and Atangana [24] to describe the dynamics of COVID-2019. They applied an Atangana-Baleanu derivative operator to their model as they believe that many properties such as the kernel which is nonlocal and non-singular, and the crossover behaviours within the model are best to explain using Atangana-Baleanu. Their results indicate that the virus is locally asymptotically stable when the reproduction less than a unit. With the given data, they estimated that the basic reproduction number for the given data is $R_0 \approx 2.4829$. The Atangana-Baleanu fractional derivative operator-based model was also used by Khan et al. in [26] in studying the dynamics of COVID-19 by incorporating the quarantine and isolations principles in the model formulations.

The exponential growth of the pandemic and chaotic situations it caused globally in the health sector, international trades, travel and tourism, as well as energy sector is undoubtedly significant, see Nuugulu et al. in [23]. The unprecedented effects of the virus have forced governments and private institutions globally to take drastic measures to contain further spread of the virus. Some of those measures implemented globally are travel restrictions, lockdowns, physical distancing and self-isolations among others. While these measures are in place, researchers around the world are now working on different theory and models to understand the dynamics of the spread and possible impact of COVID-19. The primary motivation therein is to assist the policy and decision-makers as well as health officials to plan for healthcare needs and craft out appropriate mitigation strategies as epidemic unfold.

Namibia being a semi-arid country situated in Southern Africa has also not being spared, by the time of finalising this manuscript, Namibia has recorded a total of 25 positive cases, a majority of which are all travel related. Compared to other countries in the region, Namibia has been applauded of its effective efforts in cushioning the unanticipated impacts of the outbreak. Declaration of a state of emergency on the outbreak earlier and locking down the entire country was some of the best strategies the country used in curbing further spread of the virus.

This chapter therefore firstly serves to propose a fractional calculus-based model and its robust numerical method for modelling the spread of COVID-19 in Namibia. Secondly, the study serves to illustrate why there is a need for Namibia to continue on its best trajectory in controlling and managing further spread of COVID-19 as

well as set out some policy recommendations for managing the spread of COVID-19 in the country. The rest of the chapter is organised as follows. In Sect. **Conceptual Model**, we present the conceptual model under consideration, whereas in Sect. **Mathematical Analysis of the Conceptual Model**, we carry out the analysis of the conceptual model. The numerical method is derived in Sect. **Construction of the Numerical Method** and the results and discussions are presented in Sect. **Results and Discussion**. Section **Concluding Remarks and Policy Recommendations** presents the conclusion and policy recommendations.

Conceptual Model

The model under consideration is a fractional susceptible-exposed-infected-recovered (SEIR) model. Our classes are defined as follow: susceptible (S)—those individuals who are at the risk of infection, exposed (E)—those individuals who are already exposed to the virus by being in contact with a person who is infected, infected (I)—comprising of individuals who are diagnosed and tested positive for COVID-19 and lastly the recovered individuals in class (R). Figure 9.1 shows a graphical representation of the dynamics of the considered SEIR model.

A fractional SEIR model is a generalisation of the well-known classical SEIR model. In this model, we assume that the change in the population follows a superfractal diffusion process with fractional steps characterised by the Hurst parameter $\alpha \in [1/2, 1)$. The Hurst parameter α is very fundamental in effectively modelling the chaotic nature of the spread of the COVID-19. Assuming that the incubation period is a random variable with exponential distribution with parameter ϑ (i.e., the average incubation period is ϑ^{-1}) and also assuming the presence of vital dynamics with birth rate Λ equal to death rate μ , we get the following model

$$\begin{cases} {}^c D_t^\alpha S_t = \Lambda - \mu S_t - \beta \frac{I_t}{N} S_t, \\ {}^c D_t^\alpha E_t = \beta \frac{I_t}{N} S_t - (\mu + \vartheta) E_t, \\ {}^c D_t^\alpha I_t = \vartheta E_t - (\pi + \mu) I_t, \\ {}^c D_t^\alpha R_t = \pi I_t - \mu R_t, \\ \text{with} \\ S_t(0) = S_0 \geq 0, E_t(0) = E_0 \geq 0, I_t(0) = I_0 \geq 0, R_t(0) = R_0 \geq 0, \text{ on } [0, T], \end{cases} \tag{9.1}$$

where $t \leq T \in \mathbb{R}_+, \alpha \in [1/2, 1)$, ${}^c D_t^\alpha, \Lambda, \mu, \beta, \vartheta, \pi$ denote fractional derivative in defined in the Caputo sense, influx rate, death rate, infection rate, incubation rate,

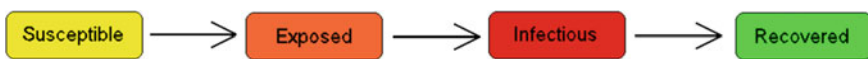


Fig. 9.1 Graphical representation of the proposed spread of COVID-19. *Source* own

recovery rate, respectively. We further assume that $N = S_t + E_t + I_t + R_t$ denotes the total population, where subscript t denotes time.

Mathematical Analysis of the Conceptual Model

In this section, we assess the existence and uniqueness of solution to (9.1), as well as its continuous dependency on data, equilibrium points, reproductive number and stability conditions.

Existence of Uniqueness of Solution and Continuously Dependency on the Data

Since the conceptual model in Eq. (9.1) is an initial value problem (IVP), it can be expressed as

$$\mathbf{u}(t) = \mathbf{u}(0) + \frac{1}{\Gamma(\alpha)} \int_0^T (t - s)^{\alpha-1} \mathbf{F}(s, \mathbf{u}(z)) ds, \tag{9.2}$$

where

$$\mathbf{u}(t) = (S_t, E_t, I_t, R_t)', \mathbf{F} = (f_1, f_2, f_3, f_4)'$$

in which,

$$\begin{cases} f_1 = \Lambda - \mu S_t - \beta \frac{I_t}{m} S_t, \\ f_2 = \beta \frac{I_t}{m} S_t - (\mu + \vartheta) E_t, \\ f_3 = \vartheta E_t - (\pi + \mu) I_t, \\ f_4 = \pi I_t - \mu R_t. \end{cases}$$

Since the IVP in Eq. (9.1) is a system of continuous functions, then it is in the space of continuous function $C[0, T]$, thus, it suffices to define the operator

$$A\mathbf{u} := \mathbf{u}(0) + \frac{1}{\Gamma(\alpha)} \int_0^T (t - s)^{\alpha-1} \mathbf{F}(s, \mathbf{u}(z)) ds, \tag{9.3}$$

such that the following results hold.

Theorem 1 *Let \mathbf{V} denote a nonempty closed subset of a Banach space \mathbb{B} , such that for every $M_j \geq 0$, $\sum_{j=0}^{\infty}$ converges. Moreover, let $A : \mathbf{V} \rightarrow \mathbf{V}$ denotes a mapping satisfying*

$$\|A^{(j)}\mathbf{u} - A^{(j)}\mathbf{v}\| \leq M_j\|\mathbf{u} - \mathbf{v}\|,$$

for every $j \in \mathbb{N}$ and $\mathbf{u}, \mathbf{v} \in \mathbf{V}$.

Proof The proof to these results has already been established in [27], therefore, we conclude that there exist a unique solution to the IVP (9.1). \square

Next, we establish results on the continuous dependency of the unique solution to the IVP in (9.1) on the data. To do so, we re-define the IVP in (9.1) as

Definition 1

$$D^\alpha(\mathbf{u} - T_0[\mathbf{u}])(t) = \mathbf{F}(t, \mathbf{u}(t)), \text{ with } \mathbf{u}(0) = \mathbf{u}_0, \tag{9.4}$$

where $T_0[\mathbf{u}]$ denotes Taylor polynomial of order 0 for \mathbf{u} centred at origin.

Theorem 2 Let $\mathcal{D} := [0, T] \times [\mathbf{u}_0 - \delta, \mathbf{u}_0 + \delta]$, for some $\delta > 0$. Furthermore, let \mathbf{u}, \mathbf{v} denote the unique solutions of

$$D^\alpha(\mathbf{u} - T_0[\mathbf{u}])(t) = \mathbf{F}(t, \mathbf{u}(t)), \text{ with } \mathbf{u}(0) = \mathbf{u}_0,$$

and

$$D^\alpha(\mathbf{v} - T_0[\mathbf{v}])(t) = \mathbf{F}(t, \mathbf{v}(t)), \text{ with } \mathbf{v}(0) = \mathbf{v}_0,$$

respectively. Then,

$$\|\mathbf{u} - \mathbf{v}\|_\infty = \mathcal{O}(\|\max |\mathbf{u}_0 - \mathbf{v}_0|\|),$$

over any compact interval in which \mathbf{u} and \mathbf{v} exist.

Lemma 1 Let $\mathcal{D} := [0, T] \times [\mathbf{u}_0 - \delta, \mathbf{u}_0 + \delta]$, for some $\delta > 0$ such that $\mathbf{F}, \tilde{\mathbf{F}}$ are continuous on \mathcal{D} and f satisfy Lipschitz conditions with respect \mathbf{u} . Furthermore, let \mathbf{u}, \mathbf{v} denote the unique solutions of

$$D^\alpha(\mathbf{u} - T_0[\mathbf{u}])(t) = \mathbf{F}(t, \mathbf{u}(t)), \text{ with } \mathbf{u}(0) = \mathbf{u}_0,$$

and

$$D^\alpha(\mathbf{v} - T_0[\mathbf{v}])(t) = \mathbf{F}(t, \mathbf{v}(t)), \text{ with } \mathbf{v}(0) = \mathbf{v}_0,$$

respectively. Then,

$$\|\mathbf{u} - \mathbf{v}\|_\infty = \mathcal{O}(\|\mathbf{F} - \tilde{\mathbf{F}}\|),$$

over any compact interval in which \mathbf{u} and \mathbf{v} exist.

Proof The proof to Theorem 2 and Lemma 1 has also been established in [27]. \square

The uniqueness and data dependency of the model on the data has been demonstrated in the two considered scenarios in Sect. Results and Discussion.

Positivity of Solution

In this section, we simply present that the solution to the IVP in equation (9.1) is biological feasible.

Theorem 3 *The IVP in Eq. (9.1) possesses positive unique solution.*

Proof In view of the total population, we see that

$${}^c D_t^\alpha N(t) = {}^c D_t^\alpha S_t + {}^c D_t^\alpha E_t + {}^c D_t^\alpha I_t + {}^c D_t^\alpha R_t,$$

which yield

$${}^c D_t^\alpha N(t) = \Lambda - \mu N \geq 0.$$

Therefore, the biological feasible region for the IVP in Eq. (9.1) is

$$\Gamma := \{(S_t, E_t, I_t, R_t) \in \mathbb{R}_+^4 : S_t, E_t, I_t, R_t \geq 0; S_t + E_t + I_t + R_t = N\}.$$

\square

Equilibrium Points

When

$${}^c D_t^\alpha S_t = {}^c D_t^\alpha E_t = {}^c D_t^\alpha I_t = {}^c D_t^\alpha R_t = 0,$$

the IVP in Eq. (9.1) yields the following results.

Theorem 4 *The fractional SEIR model (9.1) possesses at most two equilibrium points, namely the disease free equilibrium point $(\frac{\Lambda}{\mu}, 0, 0, 0)$ and an endemic equilibrium point $(S_t^*, E_t^*, I_t^*, R_t^*)$, where*

$$S_t^* = \frac{(\vartheta + \mu)(\pi + \mu)}{\beta \vartheta}, E_t^* = \left(\frac{\beta S_t^* - (\pi + \mu)}{\mu} \right) I_t^*, I_t^* = \left(\frac{\vartheta}{\pi + \mu} \right) E_t^*, R_t^* = \left(\frac{\pi \vartheta}{\pi + \mu^2} \right) E_t^*.$$

Proof In view of the third and fourth equations in Eq. (9.1), we have

$$I_t^* = \left(\frac{\vartheta}{\pi + \mu} \right) E_t^* \text{ and } R_t^* = \left(\frac{\pi}{\mu} \right) I_t^*, \tag{9.5}$$

respectively. From equations in (9.19), we obtain

$$R_t^* = \left(\frac{\pi \vartheta}{\pi + \mu^2} \right) E_t^*, \tag{9.6}$$

in which we get the following cases.

- *Case 1:* When $E_t^* = I_t^* = R_t^* = 0$.
- *Case 2:* When $E_t^* \neq 0, I_t^* \neq 0$, and $R_t^* \neq 0$.

In view of *Case 1*:, we see from the first equation one in (9.1) that

$$\Lambda - \mu S_t - \beta \frac{I_t}{N} S_t = 0, \tag{9.7}$$

whenever, ${}^c D_t^\alpha S_t = 0$, and $N_t = 1$. Solving for S_t in Eq. (9.7) we find

$$S_t^* = \frac{\Lambda}{\mu}. \tag{9.8}$$

Equation (9.8) imply that the disease free equilibrium point is $\left(\frac{\Lambda}{\mu}, 0, 0, 0 \right) \in \Gamma$.

Similarly, for *Case 2*:, we are adding the second equation to the third equation in (9.1) to get

$$(\beta S_t^* - (\pi + \mu)) I_t^* - \mu E_t^* = 0. \tag{9.9}$$

Then, substituting equation in (9.19) into equation in (9.24) and simplify further, yields

$$\beta S_t^* \vartheta = (\vartheta + \mu)(\pi + \mu),$$

which is equivalent to

$$S_t^* = \frac{(\vartheta + \mu)(\pi + \mu)}{\beta \vartheta},$$

which conclude the prove. □

Reproductive Number

We understand that the reproductive number, henceforth denoted by R_o is defined as the number of secondary cases that one case would produce in completely susceptible individuals. Therefore, to determine it from the disease free situation

$$S_t^* \geq \frac{\Lambda}{\mu}. \quad (9.10)$$

Since the endemic equilibrium S_t^* is

$$S_t^* = \frac{(\vartheta + \mu)(\pi + \mu)}{\beta\vartheta}, \quad (9.11)$$

then substituting (9.11) into (9.10) we find

$$\frac{(\vartheta + \mu)(\pi + \mu)}{\beta\vartheta} \geq \frac{\Lambda}{\mu}, \quad (9.12)$$

which is equivalent to

$$1 \geq \frac{\Lambda\beta\vartheta}{\mu(\vartheta + \mu)(\pi + \mu)}.$$

Hence, the reproductive number is

$$R_o = \frac{\Lambda\beta\vartheta}{\mu(\vartheta + \mu)(\pi + \mu)}. \quad (9.13)$$

Equation in (9.13) imply that if $R_o < 1$, the disease free equilibrium point is

$$(S_t^*, E_t^*, I_t^*, R_t^*) = \left(\frac{\Lambda}{\mu}, 0, 0, 0 \right) \geq 0,$$

whereas, if $R_o > 1$ then the endemic equilibrium point

$$(S_t^*, E_t^*, I_t^*, R_t^*) = \left(\frac{(\vartheta + \mu)(\pi + \mu)}{\beta\vartheta}, \left(\frac{\beta S_t^* - (\pi + \mu)}{\mu} \right) I_t^*, \left(\frac{\vartheta}{\pi + \mu} \right) E_t^*, \left(\frac{\pi\vartheta}{\pi + \mu^2} \right) E_t^* \right) > 0.$$

In the next section, we investigate the endemic equilibrium points with respect to R_o .

Stability Analysis

Linearising the system in Eq. (9.1) at the equilibrium point $(S_t^*, E_t^*, I_t^*, R_t^*)$, we obtain the non-zero entries of the Jacobian matrix as

$$\begin{cases} J(S_t^*, E_t^*, I_t^*, R_t^*)_{(1,1)} = -\mu - \beta I_t^*, J(S_t^*, E_t^*, I_t^*, R_t^*)_{(1,3)} = -\beta I_t^*, \\ J(S_t^*, E_t^*, I_t^*, R_t^*)_{(2,2)} = -(\mu + \vartheta), J(S_t^*, E_t^*, I_t^*, R_t^*)_{(2,3)} = \beta S_t^*, J(S_t^*, E_t^*, I_t^*, R_t^*)_{(3,2)} = \vartheta, \\ J(S_t^*, E_t^*, I_t^*, R_t^*)_{(3,3)} = -(\pi + \mu), J(S_t^*, E_t^*, I_t^*, R_t^*)_{(4,3)} = \pi, J(S_t^*, E_t^*, I_t^*, R_t^*)_{(4,4)} = -\mu. \end{cases} \quad (9.14)$$

The Jacobian matrix enables us to determine the nature of the disease free equilibrium and endemic free equilibrium. This we establish in the next section.

Stability of the Disease Free Equilibrium

At the disease free equilibrium,

$$(S_t^*, E_t^*, I_t^*, R_t^*) = \left(\frac{\Lambda}{\mu}, 0, 0, 0 \right),$$

we see that characteristic equation associated with the Jacobian matrix in Eq. (9.27) is

$$P(\lambda) = \lambda^4 + A\lambda^3 + B\lambda^2 + C\lambda + \mu^2 D, \quad (9.15)$$

where

$$\begin{cases} A = (4\mu + \pi + \vartheta), B = (3\pi\mu + \pi\vartheta - \vartheta\beta + 6\mu^2 + 3\mu\vartheta), \\ C = (3\pi\mu^2 + 2\pi\mu\vartheta - 2\vartheta\beta\mu + 4\mu^3 + 3\mu^3\vartheta), \\ D = (\pi\mu + \pi\vartheta - \vartheta\beta + \mu^2 + \mu\vartheta). \end{cases}$$

Thus, the roots of characteristic polynomials in Eq. (9.15) are

$$\begin{cases} \lambda_1 = -\mu, \lambda_2 = -\mu, \\ \lambda_3 = -\frac{\pi}{2} - \mu - \frac{\vartheta}{2} + \frac{\sqrt{\pi^2 - 2\pi\vartheta + 4\vartheta\beta + \vartheta^2}}{2} \\ \lambda_4 = -\frac{\pi}{2} - \mu - \frac{\vartheta}{2} - \frac{\sqrt{\pi^2 - 2\pi\vartheta + 4\vartheta\beta + \vartheta^2}}{2}. \end{cases} \quad (9.16)$$

Since all roots have negative real parts, it implies that a disease free equilibrium point is locally stable.

Stability of the Endemic Free Equilibrium

For the endemic free equilibrium, we obtain the following roots to the associated characteristic equation

$$\begin{cases} \lambda_1 = -\mu, \lambda_2 = -\mu - \beta \left(\frac{\Delta\beta\vartheta - \mu^3 - \mu^2\vartheta - \mu^2\pi - \mu\vartheta\pi}{\beta(\mu^2 + \mu\vartheta + \mu\pi + \vartheta\pi)} \right) \\ \lambda_3 = \frac{-\pi}{2} - \mu - \frac{\vartheta}{2} + \frac{\sqrt{\pi^2 - 2\pi\vartheta + 4\vartheta\beta\left(\frac{\vartheta + \mu}{\beta\vartheta}(\pi + \mu)\right) + \vartheta^2}}{2}, \\ \lambda_4 = \frac{-\pi}{2} - \mu - \frac{\vartheta}{2} - \frac{\sqrt{\pi^2 - 2\pi\vartheta + 4\vartheta\beta\left(\frac{\vartheta + \mu}{\beta\vartheta}(\pi + \mu)\right) + \vartheta^2}}{2}. \end{cases} \tag{9.17}$$

Since the roots of characteristic equation are real and negative with $R_o > 1$, then the endemic free equilibrium point is locally asymptotically stable. Therefore, the following results follow.

Theorem 5 *The basic reproduction number $R_o < 1$ is globally stable in the feasible region, whereas, if $R_o > 1$ the unique endemic equilibrium is globally asymptotically stable in the interior of the feasible region.*

Proof The proof to this theorem has already been established in [28]. □

Construction of the Numerical Method

In this section, we design a robust numerical scheme for solving (9.1). Let M be positive integers and define $k = T/M$ time step-size. Further denote $t_m = mk$; $m = 0, 1, 2, \dots, M$, such that $t_m \in [0, T]$, then the fractional derivatives in (9.1) can be approximated using the following numerical quadrature as formulated in [17].

We will illustrate below using initial value problem (IVP)

$$\begin{cases} {}^c D_t^\alpha S_t = f(t, S(t)), \\ S_t(0) = S_0, \end{cases} \tag{9.18}$$

where $f(t, S(t)) = \Lambda - \mu S_t - \beta \frac{I_t}{N} S_t$, the equations for the rest of the compartments will be given analogously.

$$\begin{aligned}
{}^c D_t^\alpha S_t &= \frac{1}{\Gamma(1-\alpha)} \int_0^{t_m} \frac{dS_t}{dt} (t_m - \tau)^{-\alpha} d\tau, \\
&= \frac{1}{\Gamma(1-\alpha)} \sum_{j=0}^m \int_{jk}^{(j+1)k} \left(\frac{S_{j+1} - S_j}{k} + \mathcal{O}(k) \right) (mk - \tau)^{-\alpha} d\tau, \\
&= \frac{1}{\Gamma(1-\alpha)} \sum_{j=0}^m \left(\frac{S_{j+1} - S_j}{k} + \mathcal{O}(k) \right) \left(\frac{(mk - (j+1)k)^{1-\alpha} - (mk - jk)^{1-\alpha}}{1-\alpha} \right), \\
&= \frac{1}{\Gamma(1-\alpha)} \frac{1}{1-\alpha} \sum_{j=0}^m \left(\frac{S_{j+1} - S_j}{k} + \mathcal{O}(k) \right) \left[(m-j+1)^{1-\alpha} - (m-j)^{1-\alpha} \right] k^{1-\alpha}, \\
&= \frac{1}{(\alpha-1)!} \frac{1}{k^\alpha} \sum_{j=0}^m [S_{j+1} - S_j] \left[(m-j+1)^{1-\alpha} - (m-j)^{1-\alpha} \right] \\
&\quad + \frac{1}{(\alpha-1)!} \sum_{j=0}^m \left[(m-j+1)^{1-\alpha} - (m-j)^{1-\alpha} \right] \mathcal{O}(k) k^{1-\alpha}, \\
&= \frac{1}{(\alpha-1)!} \frac{1}{k^\alpha} \sum_{j=0}^m (S_{j+1} - S_j) \left[(m-j+1)^{1-\alpha} - (m-j)^{1-\alpha} \right] \\
&\quad + \frac{1}{(\alpha-1)!} \sum_{j=0}^m \left[(m-j+1)^{1-\alpha} - (m-j)^{1-\alpha} \right] \mathcal{O}(k^{2-\alpha}). \tag{9.19}
\end{aligned}$$

Shifting the indices in (9.19), we obtain

$$\begin{aligned}
{}^c D_t^\alpha S_t &= \frac{1}{(\alpha-1)!} \frac{1}{k^\alpha} \sum_{j=0}^m (S_{j+1} - S_j) \left[(j+1)^{1-\alpha} - j^{1-\alpha} \right] \\
&\quad + \frac{1}{(\alpha-1)!} \sum_{j=0}^m \left[(j+1)^{1-\alpha} - j^{1-\alpha} \right] \mathcal{O}(k^{2-\alpha}). \tag{9.20}
\end{aligned}$$

Let,

$$\Psi := \frac{1}{(\alpha-1)!} \frac{1}{k^\alpha}, \tag{9.21}$$

and

$$\gamma_j := (j+1)^{1-\alpha} - j^{1-\alpha}; \quad j = 0, 1, \dots, m, \tag{9.22}$$

such that $1 = \gamma_0 > \gamma_1 > \dots > \gamma_m \rightarrow 0$. Substituting Ψ and γ_j into (9.20) yield

$$\begin{aligned}
 {}^c D_t^\alpha S_t &= \Psi \sum_{j=0}^m \gamma_j (S_{j+1} - S_j) + \frac{1}{(\alpha - 1)!} \sum_{j=0}^m \gamma_j \mathcal{O}(k^{2-\alpha}), \\
 &= \Psi \sum_{j=0}^m \gamma_j (S_{j+1} - S_j) + \frac{1}{(\alpha - 1)!} n^{1-\alpha} \mathcal{O}(k^{2-\alpha}), \\
 &= \Psi \sum_{j=0}^m \gamma_j (S_{j+1} - S_j) + \frac{1}{(\alpha - 1)!} \left(\frac{t_m}{k}\right)^{1-\alpha} \mathcal{O}(k^{2-\alpha}), \\
 &= \Psi \sum_{j=0}^m \gamma_j (S_{j+1} - S_j) + \frac{t_m^{1-\alpha}}{(\alpha - 1)!} k.
 \end{aligned} \tag{9.23}$$

Therefore, ${}^c D_t^\alpha S_t$ in (9.1)

$${}^c D_t^\alpha S_t = \Psi \sum_{j=0}^m \gamma_j (S_{j+1} - S_j) + \mathcal{O}(k). \tag{9.24}$$

Similarly, the rest of the compartments are

$$\begin{cases}
 {}^c D_t^\alpha E_t = \Psi \sum_{j=0}^m \gamma_j (E_{j+1} - E_j) + \mathcal{O}(k), \\
 {}^c D_t^\alpha I_t = \Psi \sum_{j=0}^m \gamma_j (I_{j+1} - I_j) + \mathcal{O}(k), \\
 {}^c D_t^\alpha R_t = \Psi \sum_{j=0}^m \gamma_j (R_{j+1} - R_j) + \mathcal{O}(k).
 \end{cases} \tag{9.25}$$

Substituting expressions in Eq. (9.24) into (9.1) and neglecting the error terms of $\mathcal{O}(k)$, equation in (9.1) simplifies to

$$\begin{cases}
 \sum_{j=0}^m \gamma_j (S_{j+1} - S_j) = \hat{\Lambda} - \hat{\mu} S_m - \hat{\beta} \frac{I_m}{N} S_m, \\
 \sum_{j=0}^m \gamma_j (E_{j+1} - E_j) = \hat{\beta} \frac{I_m}{N} S_m - (\hat{\mu} + \hat{\vartheta}) E_m, \\
 \sum_{j=0}^m \gamma_j (I_{j+1} - I_j) = \hat{\vartheta} E_m - (\hat{\pi} + \hat{\mu}) I_m, \\
 \sum_{j=0}^m \gamma_j (R_{j+1} - R_j) = \hat{\pi} I_m - \hat{\mu} R_m,
 \end{cases} \tag{9.26}$$

whereby $\hat{\Lambda} = \frac{\Lambda}{\Psi}$, $\hat{\mu} = \frac{\mu}{\Psi}$, $\hat{\beta} = \frac{\beta}{\Psi}$, $\hat{\vartheta} = \frac{\vartheta}{\Psi}$, $\hat{\pi} = \frac{\pi}{\Psi}$.

By expanding the left hand-side of (9.26), and shifting indices yield to

$$\begin{cases} \sum_{j=0}^m \gamma_j (S_{j+1} - S_j) = S_{m+1} - \gamma_m S_0 + \sum_{j=0}^{m-1} \varphi_j S_{m-j}, \\ \sum_{j=0}^m \gamma_j (E_{j+1} - E_j) = E_{m+1} - \gamma_m E_0 + \sum_{j=0}^{m-1} \varphi_j E_{m-j}, \\ \sum_{j=0}^m \gamma_j (I_{j+1} - I_j) = I_{m+1} - \gamma_m I_0 + \sum_{j=0}^{m-1} \varphi_j I_{m-j}, \\ \sum_{j=0}^m \gamma_j (R_{j+1} - R_j) = R_{m+1} - \gamma_m R_0 + \sum_{j=0}^{m-1} \varphi_j R_{m-j}, \end{cases} \quad (9.27)$$

where $\varphi_j = \gamma_j - \gamma_{j+1}$, $j = 0, 1, \dots, m$.

Remark 1 The following observations are trivial to show.

$$\begin{cases} 1 = \gamma_0 > \gamma_1 > \dots > \gamma_m \rightarrow 0, \\ \varphi_0 = 1 - \gamma_1, \\ \sum_{j=0}^{m-1} \varphi_j = 1 + \gamma_m, \\ \sum_{j=0}^{\infty} \varphi_j = 1 > 1 - (2^{1-\alpha} - 1^{1-\alpha}) = 2 - 2^{1-\alpha} = \varphi_0 > \varphi_1 > \dots \rightarrow 0. \end{cases} \quad (9.28)$$

The $\sum_{j=0}^{m-1}(\cdot)$ components in (9.27) represent the long memory effects in the COVID-19 data, which is justified by the dependence between new and the existing cases. Therefore, substituting (9.27) into (9.26) yield

$$\begin{cases} S_{m+1} = \gamma_m S_0 + \hat{\Lambda} - \hat{\mu} S_m - \hat{\beta} \frac{I_m}{N} S_m - \sum_{j=0}^{m-1} \varphi_j S_{m-j}, \\ E_{m+1} = \gamma_m E_0 + \hat{\beta} \frac{I_m}{N} S_m - (\hat{\mu} + \hat{\nu}) E_m - \sum_{j=0}^{m-1} \varphi_j E_{m-j}, \\ I_{m+1} = \gamma_m I_0 + \hat{\nu} E_m - (\hat{\pi} + \hat{\mu}) I_m - \sum_{j=0}^{m-1} \varphi_j I_{m-j}, \\ R_{m+1} = \gamma_m R_0 + \hat{\pi} I_m - \hat{\mu} R_m - \sum_{j=0}^{m-1} \varphi_j R_{m-j}. \end{cases} \quad (9.29)$$

Equation (9.29) can be expanded into

$$\begin{cases} S_{m+1} = \gamma_m S_0 + \hat{\Lambda} - \varphi_0 \hat{\mu} S_m - \hat{\beta} \frac{I_m}{N} S_m - (\varphi_1 S_{m-1} + \dots + \varphi_{m-2} S_2 + \varphi_{m-1} S_1), \\ E_{m+1} = \gamma_m E_0 + \hat{\beta} \frac{I_m}{N} S_m - (\hat{\mu} + \hat{\nu} + \varphi_0) E_m - (\varphi_1 E_{m-1} + \varphi_2 E_{m-2} \dots + \varphi_{m-2} E_2 + \varphi_{m-1} E_1), \\ I_{m+1} = \gamma_m I_0 + \hat{\nu} E_m - (\hat{\pi} + \hat{\mu} + \varphi_0) I_m - (\varphi_1 I_{m-1} + \varphi_2 I_{m-2} \dots + \varphi_{m-2} I_2 + \varphi_{m-1} I_1), \\ R_{m+1} = \gamma_m R_0 + \hat{\pi} I_m - (\hat{\mu} - \varphi_0) R_m - (\varphi_1 R_{m-1} + \varphi_2 R_{m-2} \dots + \varphi_{m-2} R_2 + \varphi_{m-1} R_1). \end{cases} \quad (9.30)$$

The above scheme (9.30) was implemented as an iterative process using MATLAB.

Analysis of the Numerical Method

The exact solution of this problem is not available and in order to calculate the maximum pointwise error and rate of convergence, we use the double mesh principle. We define the double mesh principle as follow;

$$\epsilon_C^M = \max_{x_j \in \bar{D}_C^M} |U^M(x_j) - U^{2M}(x_j)|, \quad (9.31)$$

and

$$\epsilon_C^M = \max_C \epsilon_C^M, \quad (9.32)$$

where \bar{D}_C^M is the domain with $U^M(x_j)$ and $U^{2M}(x_j)$ denoting numerical solutions obtained using M and $2M$ mesh intervals, respectively (Table 9.1).

Furthermore, the robust orders of convergence are computed using

$$r = \log_2 \left(\frac{\epsilon_C^M}{\epsilon_C^{2M}} \right). \quad (9.33)$$

We will use (9.32) and (9.33), respectively, to compute the maximum absolute errors and orders of convergence of the numerical scheme in (9.30). The stability and convergence results to the two scenarios presented in Sect. [Results and Discussion](#) are appearing in Tables 9.2, 9.3, 9.5, 9.6 and 9.4.

Table 9.1 Parameter values for Example 1

Birth rate (λ)	Death rate (μ)	Infection rate (β)	Incubation period ($1/\vartheta$)	Recovery rate (π)
0.013	0.013	0.06	14	0.98

source own

Table 9.2 Maximum absolute errors for Example 1 with $\Lambda = 0.013, \mu = 0.013, \beta = 0.06, 1/\vartheta = 14$ and $\pi = 0.98$

α	$M = 100$	$M = 200$	$M = 400$	$M = 800$	$M = 1600$
0.1	6.1152e-02	3.1069e-02	1.5659e-02	7.8606e-03	3.9381e-03
0.2	5.9707e-02	3.0276e-02	1.5245e-02	7.6491e-03	3.8312e-03
0.3	5.7925e-02	2.9330e-02	1.4758e-02	7.4021e-03	3.7069e-03
0.4	5.5896e-02	2.8272e-02	1.4218e-02	7.1294e-03	3.5698e-03
0.5	5.3692e-02	2.7136e-02	1.3641e-02	6.8388e-03	3.4240e-03
0.6	5.1370e-02	2.5948e-02	1.3040e-02	6.5369e-03	3.2726e-03
0.7	4.8978e-02	2.4731e-02	1.2427e-02	6.2289e-03	3.1183e-03
0.8	4.6552e-02	2.3503e-02	1.1809e-02	5.9190e-03	2.9631e-03
0.9	4.4121e-02	2.2277e-02	1.1194e-02	5.6107e-03	2.8088e-03
1.0	4.1705e-02	2.1064e-02	1.0586e-02	5.3066e-03	2.6567e-03

Source own

Table 9.3 Convergence rates for Example 1 with $\Lambda = 0.013, \mu = 0.013, \beta = 0.06, 1/\vartheta = 14$ and $\pi = 0.98$

α	$M = 200$	$M = 400$	$M = 800$	$M = 1600$
0.1	0.98	0.99	0.99	1.00
0.2	0.98	0.99	0.99	1.00
0.3	0.98	0.99	1.00	1.00
0.4	0.98	0.99	1.00	1.00
0.5	0.98	0.99	1.00	1.00
0.6	0.99	0.99	1.00	1.00
0.7	0.99	0.99	1.00	1.00
0.8	0.99	0.99	1.00	1.00
0.9	0.99	0.99	1.00	1.00
1.0	0.99	0.99	1.00	1.00

Source own

Table 9.4 Parameter values for Example 1

Birth rate (λ)	Death rate (μ)	Infection rate (β)	Incubation period ($1/\vartheta$)	Recovery rate (π)
0.023	0.023	0.10	7	0.70

Source own

Table 9.5 Maximum absolute errors for Example 1 with $\Lambda = 0.023, \mu = 0.023, \beta = 0.10, 1/\vartheta = 7$ and $\pi = 0.70$

α	$M = 100$	$M = 200$	$M = 400$	$M = 800$	$M = 1600$
0.1	1.5661e-01	8.1330e-02	4.1509e-02	2.0978e-02	1.0547e-02
0.2	1.3930e-01	7.2084e-02	3.6713e-02	1.8533e-02	9.3120e-03
0.3	1.2548e-01	6.4751e-02	3.2926e-02	1.6607e-02	8.3404e-03
0.4	1.1445e-01	5.8938e-02	2.9934e-02	1.5088e-02	7.5750e-03
0.5	1.0574e-01	5.4365e-02	2.7586e-02	1.3898e-02	6.9759e-03
0.6	9.8970e-02	5.0832e-02	2.5777e-02	1.2983e-02	6.5152e-03
0.7	9.3914e-02	4.8203e-02	2.4435e-02	1.2304e-02	6.1741e-03
0.8	9.0418e-02	4.6397e-02	2.3516e-02	1.1840e-02	5.9410e-03
0.9	8.8420e-02	4.5378e-02	2.3001e-02	1.1581e-02	5.8109e-03
1.0	8.7951e-02	4.5161e-02	2.2896e-02	1.1530e-02	5.7857e-03

Source own

Table 9.6 Convergence rates for Example 1 with $\Lambda = 0.023, \mu = 0.023, \beta = 0.10, 1/\vartheta = 7$ and $\pi = 0.70$

α	$M = 200$	$M = 400$	$M = 800$	$M = 1600$
0.1	0.95	0.97	0.98	0.97
0.2	0.95	0.97	0.99	0.99
0.3	0.95	0.98	0.99	0.99
0.4	0.96	0.98	0.99	0.99
0.5	0.96	0.98	0.99	0.99
0.6	0.96	0.98	0.99	0.98
0.7	0.97	0.98	0.99	0.99
0.8	0.97	0.98	0.99	0.99
0.9	0.97	0.98	0.99	0.99
1.0	0.97	0.98	0.99	0.99

Source own

Results and Discussion

In this section, we consider two scenarios of the spread of COVID-19 in Namibia. In Example 1, we consider a case when proper quarantining, and lockdown regulations are followed and in Example 1, we consider a case where the government does not effectively implement and enforce the quarantining protocols to those individuals who travelled from outside the country, for example, truck drivers and essential goods suppliers. Apart from the opening of the Namibian borders to essential goods and services providers to and from Namibia, the proposition of Example 1 was also necessitated by the envisaged opening of Namibian borders to tourists by July 2020. These two reasons are believed to be key risk factors to importation of COVID-19 infections into the country. The projections herein are made from July 2020 up to

July 2021 under the condition that no effective and affordable vaccine or cure for COVID-19 is made available until then.

To simulate our model under the two considered scenarios, the generic initial conditions to the model are that the susceptible population is the country's entire population, i.e. ($S_0 = 2, 200, 000$ people), exposed individuals ($E_0 = 1680$ people), infected individuals ($I_0 = 202$ people) and recovered individuals ($R_0 = 27$ people).

Remark 1 In this scenario, the following model parameters were used, birth rate ($\Lambda = 0.013$), death rate ($\mu = 0.013$), infection rate ($\beta = 0.06$), incubation period ($1/\vartheta = 14$) and recovery rate ($\pi = 0.98$).

Example 1 In this scenario, we assume the violation of established quarantine protocols, inconsistencies in management of positive cases, no proper contact tracing and early isolations. With these assumptions in place, the following model parameters were used, birth rate ($\Lambda = 0.023$), death rate ($\mu = 0.023$), infection rate ($\beta = 0.10$), incubation period ($1/\vartheta = 7$) and recovery rate ($\pi = 0.70$).

General results as observed in Figs. 9.2 and 9.4 indicate that the fractional calculus approach proposed in this chapter is highly predictive for when $0 < \alpha \leq 0.5$ and conservative when $0.5 < \alpha < 1$. These observations substantiate the use of fractional order derivatives over full order derivatives. From the numerical point of view, when $0.5 < \alpha < 1$ the order of the fractional derivative operator is more closer or equal to unit, in which case, we have a classical SEIR model. Whereas, when $0 < \alpha \leq 0.5$, we have super-diffusive fractal dynamics characterised by persistent non-Gaussian increments in the underlying process with memory (Figs. 9.2 and 9.4).

In order to show how convergent, stable and robust, the proposed method is in solving the fractional SEIR model presented in (9.1), we present the numerical stability and convergence results in Tables 9.2 and 9.3 for Example 1, as well as Tables 9.5 and 9.6 for Example 1. These results were computed using the double mesh principle described in Sect. Analysis of the Numerical Method. As one can see from the results presented in Tables 9.2 and 9.5, the proposed method is very robust and unconditionally stable for a range of values of α ($0 < \alpha \leq 1$). The results in Tables 9.3 and 9.6 further indicate that indeed the numerical method is convergent with order ($\mathcal{O}(1)$). Therefore, from the numerical point of view, the fact that the method is unconditionally stable, α can be chosen to be small or large without affecting the order of accuracy the proposed method.

Furthermore, from the application point of view, results from the best case scenario presented in Example 1 indicate that given current (as of 11 July 2020) statistics, if the government continue to exercise proper quarantining of individuals coming from affected countries, isolating the infected individuals, timely tracing contacts of the infected individuals, as well as heavily investing in public health awareness campaigns to sensitise the general public on the danger and impact of COVID-19 to the country, then, the spread of the virus can be reasonably contained at around 1800 positive cases by October 2020. It is further projected in Fig. 9.3a that secondary cases may raise from 10 to around 60 cases from July 2020 and will subside by October 2020 and that the mortality rate will remain substantially below 3% of the infected cases under the same reporting period (see Fig. 9.3b).

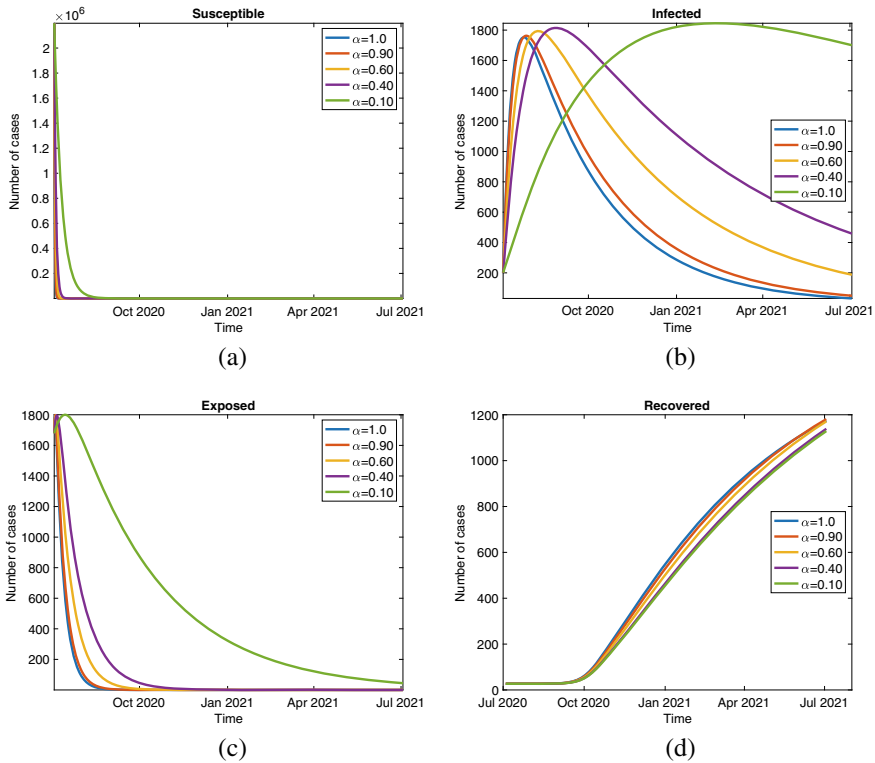


Fig. 9.2 Numerical solution to Eq. (9.1) under Example 1: **a** susceptible population, **b** infected population, **c** exposed population and **d** recovered population at different values of α . Model parameter values are given in Table 9.1. *Source* own

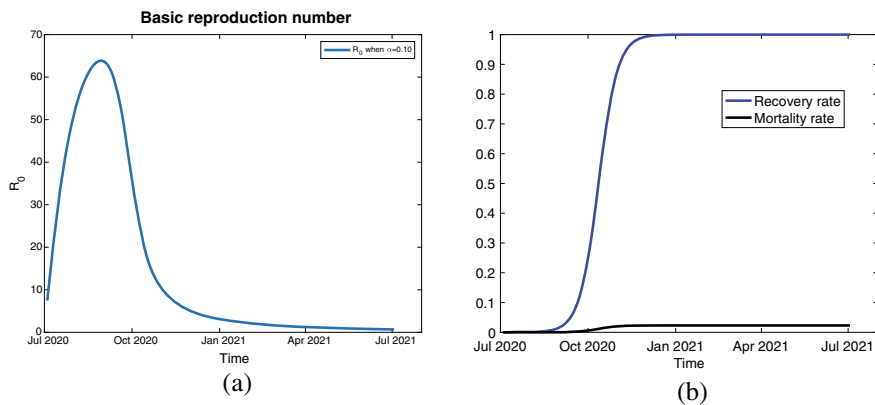


Fig. 9.3 **a** R_0 and **b** projected recovery and mortality rate under Example 1 at $\alpha = 0.10$ for model parameters under Table 9.1. *Source* own

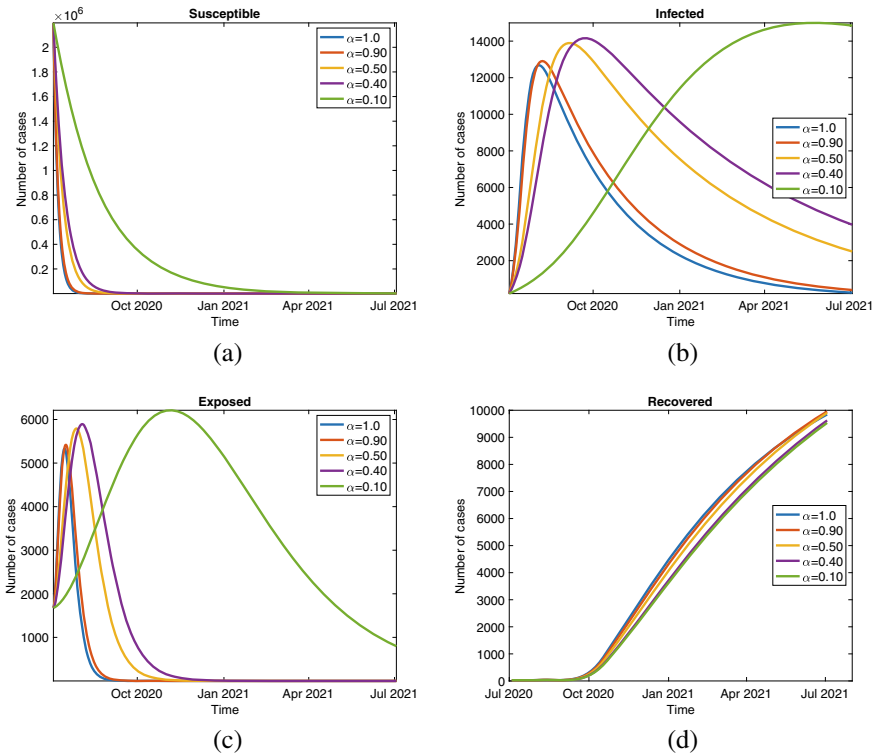


Fig. 9.4 Numerical solution to Eq. (9.1) under Example 1: **a** susceptible population, **b** infected population, **c** exposed population and **d** recovered population at different values of α . Model parameter values are given in Table 9.4. *Source* own

Moreover, if the Namibian government reinforce its efforts in kerbing further spread of the virus, secondary cases are projected to reach zero by July 2021, see Fig. 9.3a and also that by the end of 2020, a very significant proportion of the existing positive cases would have recovered and further spread substantially contained, see Fig. 9.2d. The overall mortality rate as projected in Figs. 9.3b and 9.5b for both scenarios will remain way below a 3% level for the period under investigation.

In the worse-case scenario under Example 1, given the current reported trend of widespread community transmission across the country, our results indicate that if government does not take drastic steps to kerb further community transmissions in major regions of the country, namely Khomas, Erongo as well as a majority of northern regions where a few cases of local transmissions have been reported, and Namibia can potential record over 14, 000 cases of positive COVID-19 infections in a very short period of time, see Fig. 9.4. In the absence of an effective cure or vaccine for COVID-19, our projections will remain valid.

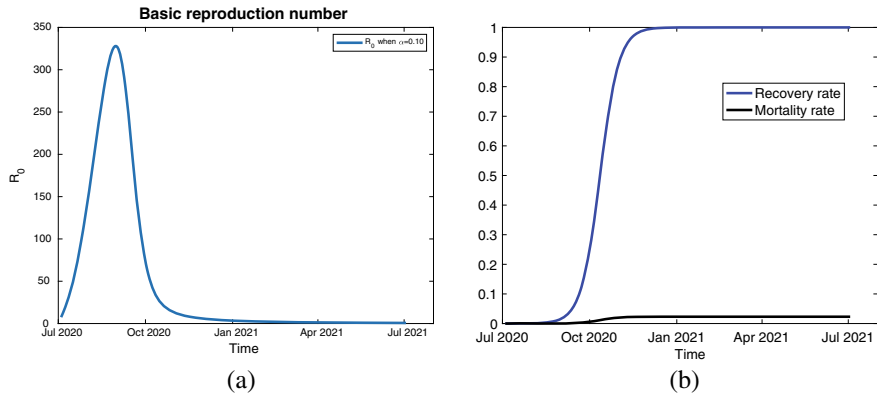


Fig. 9.5 **a** R_0 and **b** projected recovery and mortality rate under Example 1 at $\alpha = 0.10$ for model parameters under Table 9.4. *Source* own

Concluding Remarks and Policy Recommendations

Though Namibia did not record any cases of local transmission up until May 2020, the number of positive cases has been on an increase on a daily basis. In this chapter, a fractional SEIR model and its robust first-order unconditionally convergent numerical method is proposed. Results herein indicate that the fractional calculus approach and the numerical method used are well appropriate for modelling the dynamics of the spread of COVID-19. From the numerical point of view, the results indicate that the considered method is robust and unconditionally converges with order 1. From the application point of view, we considered two scenarios characterised by different parameterisation of the fractional SEIR model. The first scenario is regarded as the best case scenario, which is characterised by proper quarantining protocols, effective contact tracing and isolation of positive individuals and their contacts. In the second scenario, we looked at a worst-case scenario characterised by ineffective quarantining and isolation procedures, non-compliance of the general public to the set guidelines for kerbing the spread of the virus and enforcement of the set guidelines by the relevant assigned authorities. The two considered scenarios present similar structural features in terms of profiling the three compartments of the considered SEIR model. However, the spread of the virus is amplified in the worst-case scenario with longer delays in the recovery of the infected individuals.

In an effort to help isolate and kerb further spread of the virus, this current work draws some policy recommendations:

1. It is recommended that government revert back to stage 1 of the declaration of a national health emergency on COVID-19, at least for a period of 14 days in those regions with a high community transmission.
2. Enforce working from home for non-essentially entities.

3. Alcohol outlets should only open on a takeaway basis until a point where the country has attained a full control of the virus.
4. Furthermore, it is recommended that schools and high education institutions should take their teaching and learning to 100% e-learning at least for the remainder for the current academic year 2020.
5. Those schools which are unable to offer their classes online should be allowed to cancel the current academic year.

Acknowledgements The authors would like to thank the two anonymous reviewers whose comments and suggestions helped improve this chapter.

References

1. Djilali, S., & Ghanbari, B. (2020). Coronavirus pandemic: A predictive analysis of the peak outbreak epidemic in South Africa. *Turkey, and Brazil, Chaos, Solitons & Fractals*, *138*, 109971.
2. Mishra, A. M., Purohit, S. D., Owolabi, K. M., & Sharma, Y. D. (2020). A nonlinear epidemiological model considering asymptotic and quarantine classes for SARS CoV-2 Virus. *Chaos, Solitons & Fractals*, *138*, 109953.
3. Hu, Y., Sun, J., Dai, Z., Deng, H., Li, X., Huang, Q., et al. (2020). Prevalence and severity of corona virus disease 2019 (COVID-19): A systematic review and meta-analysis. *Journal of Clinical Virology*, *127*, 104371.
4. Postnikov, E. B. (2020). Estimation of COVID-19 dynamics “on a back-of-envelope”: Does the simplest SIR model provide quantitative parameters and predictions? *Chaos, Solitons & Fractals*, *135*, 109841.
5. Manotosh, M., Soovoojeet, J., Swapan, K. N., Anupam, K., Sayani, A., & Kar, T. K. (2020). A model based study on the dynamics of COVID-19: Prediction and control. *Chaos, Solitons & Fractals*, *136*, 109889.
6. Kassa, S. M., Njagarah, J. B. H., & Terefe, Y. A. (2020). Analysis of the mitigation strategies for COVID-19: From mathematical modelling perspective. *Chaos, Solitons & Fractals*, *138*, 109968.
7. Fanelli, D., & Piazza, F. (2020). Analysis and forecast of COVID-19 spreading in China. *Italy and France, Chaos, Solitons & Fractals*, *134*, 109761.
8. Ullah, S., & Khan, M. A. (2020). Modeling the impact of non-pharmaceutical interventions on the dynamics of novel coronavirus with optimal control analysis with a case study, *Chaos, Solitons & Fractals*, *139*, 110075. <https://doi.org/10.1016/j.chaos.2020.110075>.
9. Barmparis, G. D., & Tsironis, G. P. (2020). Estimating the infection horizon of COVID-19 in eight countries with a data-driven approach. *Chaos, Solitons & Fractals*, *135*, 109842.
10. Willis, M. J., Díaz, V. H. G., Prado-Rubio, O. A., & von Stosch, M. (2020). Insights into the dynamics and control of COVID-19 infection rates, *Chaos, Solitons & Fractals*, *138*, 109937.
11. Amina, R., Shah, K., Asifa, M., Khana, I., & Ullaha, F. (2020). An efficient algorithm for numerical solution of fractional integro-differential equations via Haar wavelet. *Journal of Computational and Applied Mathematics*, *381*, 113028.
12. Alzaid, S. S., & Alkahtani, B. S. T. (2019). Modified numerical methods for fractional differential equations. *Alexandria Engineering Journal*, *58*, 1439–1447.
13. Al-Zhour, Z., Al-Mutairi, N., Alrawajeh, F., & Alkhasawneh, R. (2019). Series solutions for the Laguerre and Lane-Emden fractional differential equations in the sense of conformable fractional derivative. *Alexandria Engineering Journal*, *58*, 1413–1420.
14. Das, S. (2008). *Functional Fractional Calculus for System Identification and Controls*. Berlin, Heidelberg: Springer-Verlag.

15. Alkahtani, B. S. T., & Alzaid, S. S. (2020). A novel mathematics model of covid-19 with fractional derivative. *Stability and Numerical Analysis, Chaos, Solitons & Fractals*, 138, 110006.
16. Atangana, A. (2020). Modelling the spread of COVID-19 with new fractal-fractional operators: Can the lockdown save mankind before vaccination. *Chaos, Solitons & Fractals*, 136, 3109860.
17. Nuugulu, S.M., Gideon, F. & Patidar, K. C. (2020). A robust θ -method for a time-space-fractional black-scholes equation, *Springer Proceedings, Article in Press*.
18. Nuugulu, S. M., Gideon, F., & Patidar, K. C. (2020). *An efficient finite difference approximation for a time-fractional black-scholes PDE arising via fractal market hypothesis*. Under Review: Alexandria Engineering Journal.
19. Owolabi, K. M. (2019). Mathematical modelling and analysis of love dynamics: A fractional approach. *Physica A*, 525, 849–865.
20. Prakash, A., & Kaur, H. (2019). Analysis and numerical simulation of fractional order Cahn-Allen model with Atangana-Baleanu derivative. *Chaos, Solitons & Fractals*, 124, 134–142.
21. Nuugulu, S. M., Gideon, F., & Patidar, K. C. (2020). *An efficient numerical method for pricing double barrier options on an underlying asset following a fractal stochastic process*. Under Review: Applied and Computational Mathematics.
22. Nuugulu, S. M., Gideon, F., & Patidar, K. C. (2020). *A robust numerical scheme for a time fractional Black-Scholes partial differential equation describing stock exchange dynamics*, *Chaos, Solitons & Fractals*: Article In Press.
23. Julius, E. T., Nuugulu, S. M., & Julius L. H. (2020). Estimating the economic impact of Covid-19: a case study of Namibia, *MPRA* (preprint) <https://mpra.ub.uni-muenchen.de/99641/>.
24. Khan, M. A., & Atangana, A. (2020). Modeling the dynamics of novel coronavirus (2019-nCov) with fractional derivative. *Alexandria Engineering Journal*, 59, 2379–2389. <https://doi.org/10.1016/j.aej.2020.02.033>.
25. Zhang, Y., Yu, X., Sun, H., Tick, G. R., Wei, W., & Jin, B. (2020). Applicability of time fractional derivative models for simulating the dynamics and mitigation scenarios of COVID-19. *Chaos, Solitons & Fractals*, 138, 109959.
26. Khan, M. A., Atangana, A., Alzahrani, E., & Fatmawati, E. (2020). The dynamics of COVID-19 with quarantined and isolation. *Advances in Difference Equations*, 1, 425. <https://doi.org/10.1186/s13662-020-02882-9>.
27. Diethelm, K., & Ford, N. J. (2002). Analysis of fractional differential equations. *Journal of Mathematical Analysis and Applications*, 265, 229–248.
28. Li, M. Y., & Wang, L. (2020). Global stability in some seir epidemic models. *The IMA Volumes in Mathematics and its Applications* 126. (2002) (Springer, New York)